

A Gradient-Enhanced Continuum Damage Model for Residually Stressed Fibre-Reinforced Materials at Finite Strains

Tobias Waffenschmidt, César Polindara and Andreas Menzel

Abstract The modelling of damage effects in materials constitutes a major challenge in various engineering-related disciplines. However, the assumption of purely *local* continuum damage formulations may lead to ill-posed boundary value problems and—with regard to numerical methods such as the finite element method—to mesh-dependent solutions, a vanishing localised damage zone upon mesh refinement, and hence physically questionable results. In order to circumvent these deficiencies, we present a *non-local gradient-enhanced* damage model at finite strains. We additionally compose the hyperelastic constitutive response at local material point level of an isotropic matrix and of an anisotropic fibre-reinforced material. The inelastic constitutive response is characterised by a scalar $[1-d]$ -damage model, where we assume only the anisotropic elastic part to damage. Furthermore, we enhance the local free energy by a gradient-term. This term essentially contains the gradient of the non-local damage variable which we introduce as an additional global field variable. In order to guarantee the equivalence between the local and non-local damage variable, we incorporate a penalisation term within the free energy. Based on the principle of minimum total potential energy, we obtain a coupled system of variational equations. The associated non-linear system of equations is symmetric and can conveniently be solved by standard incremental-iterative Newton-Raphson schemes or arc-length-based solution methods. As a further key aspect, we incorporate *residual stresses* by means of a multiplicative composition of the deformation gradient. As a three-dimensional finite element example, we study the material degradation of a fibre-reinforced tube subjected to internal pressure. This highlights the mesh-objective and constitutive properties of the model and illustratively underlines the capabilities of the formulation with regard to biomechanical application such as the simulation of arteries.

Keywords Gradient-enhanced damage · Large deformations · Finite element method · Residual stresses · Anisotropic biological tissues

T. Waffenschmidt (✉) · C. Polindara · A. Menzel

Department of Mechanical Engineering, Institute of Mechanics, Technical University Dortmund,
Leonhard-Euler-Str. 5, 44227 Dortmund, Germany
e-mail: tobias.waffenschmidt@udo.edu

A. Menzel

Division of Solid Mechanics, Lund University, P.O. Box 118, SE-22100 Lund, Sweden

© Springer International Publishing Switzerland 2015

T. Lenarz and P. Wriggers (eds.), *Biomedical Technology*, Lecture Notes

in Applied and Computational Mechanics 74, DOI 10.1007/978-3-319-10981-7_2

1 Introduction

The physical understanding and modelling of damage and failure in materials presents a major challenge in various engineering-related disciplines. To give an example, the modelling of damage effects in anisotropic soft biological tissues is closely related to the continuous failure of fibres embedded in the ambient matrix material. Arteries, for instance, can be considered as a composite of an isotropic ground substance of elastin fibres and a highly anisotropic network of cross-linked collagen fibrils. Mechanical loading beyond the physiological loading range, e.g. caused by a surgical intervention such as balloon angioplasty, can significantly reduce the elastic properties of the artery. These softening phenomena can be attributed to the continuous overstretch and degradation of particular collagen fibres.

Based on the classical work by Kachanov [8], who associated damage effects to an area reduction of the stress-bearing region, material degradation can be modelled by means of standard continuum damage formulations, i.e. in a local sense. Up to now, a large variety of models exist where we refer the reader to classic monographs and textbooks as, e.g. Krajcinovic and Lemaitre [9], or Lemaitre [10], to name only two. However, the assumption of a purely *local* continuum damage may imply the ill-posedness of the underlying boundary value problem. With regard to numerical methods such as the finite element method, this may lead to mesh-dependent solutions, a vanishing localised damage zone upon mesh refinement, and hence physically questionable results.

In order to circumvent these deficiencies, i.e. to *regularise* the problem, several approaches have been proposed in the literature as, for instance, the concept of generalised *non-local* continua, where internal length scales are introduced into the continuum formulation, see the monograph by Eringen [4], the article by Aifantis [1] or the contributions in Eringen [3] and Rogula [13]. A non-local continuum formulation can generally be established by either introducing an integral- or a gradient-type equation.

In this contribution, we apply a non-local gradient-based damage formulation within a geometrically non-linear setting allowing for large deformations. Conceptually following Dimitrijević and Hackl [2], we enhance the local free energy by a gradient-term. This term essentially contains the gradient of the non-local damage variable which, itself, is introduced as an additional global field variable. In order to guarantee the equivalence between the local and non-local damage variable, a penalisation term is incorporated within the free energy. Based on the principle of minimum total potential energy, a coupled system of Euler-Lagrange equations, i.e. the balance of linear momentum and the balance corresponding to the non-local damage field, is obtained and solved in weak form. As a key aspect, the hyper-elastic constitutive response at local material point level is governed by a highly non-linear strain energy, additively composed of an isotropic matrix material and of an anisotropic contribution related to the fibre-reinforcement. The inelastic constitutive response is represented by a scalar $[1-d]$ -damage formulation, where only the anisotropic elastic part is assumed to damage. The resulting coupled, highly

non-linear system of equations is symmetric and can conveniently be solved by standard incremental-iterative Newton-Raphson schemes or arc-length-based solution methods without any need for advanced and computationally expensive solution methods such as a global active-set-search as applied by Liebe et al. [11]. Furthermore, the approach proves to be robust, even at high levels of degradation, and allows to incorporate any suitable scalar-valued damage formulation.

Apart from the highly nonlinear elastic response of soft biological tissues, it is well-known that the structural design of arteries is characterised by a fibre-reinforced multi-layered composite subjected to pronounced *residual stresses*. The complex interaction of material properties with these residual stress effects and the geometry guarantees the optimal support under different blood pressures within the vessel. As a further key aspect of this contribution, we therefore incorporate residual stresses by means of a multiplicative composition of the deformation gradient.

This article is structured as follows: In Sect. 2, we summarise relevant kinematic relations for the geometrically non-linear case and the balance equations of the coupled boundary value problem in weak form. In Sect. 3, we specify the underlying constitutive equations, containing the isotropic and anisotropic non-linear elastic and gradient-enhanced free energies, as well as the continuum damage formulation. In Sect. 4, we discretise the governing weak forms by means of the finite element method resulting in a coupled non-linear system of equations. Last, in Sect. 6, we apply the model to illustrative three-dimensional inhomogeneous deformation problems. In order to show the capabilities of the approach with regard to biomechanics-related problems, we study a force-driven finite element example by means of an anisotropic artery-like tube subjected to internal pressure and under consideration of residual stresses. We conclude with a summary and future perspectives in Sect. 7.

2 Gradient Enhancement of a Continuum Damage Formulation

This section summarises the essential kinematic relations and presents the governing coupled balance equations of the boundary value problem on the basis of the principle of minimum total potential energy. The related variational form provides the basis for the finite element discretisation described in Sect. 4.

2.1 Basic Kinematics

Let $\mathbf{x} = \boldsymbol{\varphi}(X, t)$ describe the deformation of the body, which transforms referential placements $X \in \mathcal{B}_0$ to their spatial counterparts $\mathbf{x} \in \mathcal{B}_t$. Based on this, the deformation gradient is defined as $\mathbf{F} = \nabla_X \boldsymbol{\varphi}$ which transforms infinitesimal referential line elements dX onto their spatial counterparts $d\mathbf{x}$. Furthermore, let dV and dv denote

an infinitesimal volume element in referential and spatial setting. Accordingly, the Jacobian $J = dv/dV = \det(\mathbf{F}) > 0$ is the ratio of the deformed to the undeformed volume. Finally, let $d\mathbf{A} = \mathbf{N} dA$ and $d\mathbf{a} = \mathbf{n} da$ define the referential and spatial area normals. Then, Nanson's formula $\mathbf{n} da = \text{cof}(\mathbf{F}) \cdot \mathbf{N} dA$ describes the transformation of infinitesimal area elements between the reference and the spatial configuration with the co-factor of \mathbf{F} defined as $\text{cof}(\mathbf{F}) = J\mathbf{F}^{-t}$. Fibre-reinforcement of the material is incorporated by assuming two families of fibres to be embedded in the continuum. Their orientation is characterised by referential unit vectors \mathbf{a}_{0i} , $i = 1, 2$ with $\|\mathbf{a}_{0i}\| = 1$.

2.2 General Gradient-Enhanced Format of the Free Energy

We assume the local free energy

$$\Psi_{\text{loc}}(\mathbf{F}, \mathbf{a}_{0i}, \kappa) = \Psi_{\text{iso}}(\mathbf{F}) + f_d(\kappa) \Psi_{\text{ani}}(\mathbf{F}, \mathbf{a}_{0i}) \quad (1)$$

to account for anisotropic non-linear elastic material response under the influence of scalar damage. Basically, we additively compose the effective free energy of the undamaged material of an isotropic contribution Ψ_{iso} representing the ground substance and of an anisotropic contribution Ψ_{ani} associated with i fibre families. We assume only the anisotropic part to be affected by the damage, whereas the isotropic matrix material remains elastic. In Eq. (1), $\kappa \in [0, \infty)$ is a scalar internal damage variable, characterising a material stiffness loss of the fibres, while $f_d(\kappa) = 1 - d \in (0, 1]$ represents an appropriate damage function that is at least twice differentiable and satisfies $f_d(0) = 1$ and $f_d(\kappa \rightarrow \infty) \rightarrow 0$. This ensures purely elastic behaviour of the undamaged material and complete loss of the related material stiffness for $\kappa \rightarrow \infty$. Conceptually following the approach by Dimitrijević and Hackl [2], we introduce a gradient-enhanced non-local free energy Ψ_{nloc} as

$$\Psi_{\text{nloc}}(\phi, \nabla_X \phi, \kappa; \mathbf{F}) = \Psi_{\text{grd}}(\nabla_X \phi; \mathbf{F}) + \Psi_{\text{plty}}(\phi, \kappa). \quad (2)$$

Here, Ψ_{grd} contains the referential gradient of the non-local damage field variable ϕ while Ψ_{plty} incorporates a penalisation term which links the non-local damage variable ϕ to the local damage variable κ . Consequently, we obtain an enhanced free energy as

$$\Psi_{\text{int}}(\mathbf{F}, \phi, \nabla_X \phi, \mathbf{a}_{0i}, \kappa) = \Psi_{\text{loc}}(\mathbf{F}, \mathbf{a}_{0i}, \kappa) + \Psi_{\text{nloc}}(\phi, \nabla_X \phi, \kappa; \mathbf{F}). \quad (3)$$

Provided that the external load can be derived from a potential, we can specify the local external energy function as $\Psi_{\text{ext}}(\boldsymbol{\varphi})$. In summary, the total potential energy function is additively composed of the internal and external contribution so that its

local form reads

$$\Psi(\boldsymbol{\varphi}, \mathbf{F}, \phi, \nabla_X \phi, \mathbf{a}_{0i}, \kappa) = \Psi_{\text{int}}(\mathbf{F}, \phi, \nabla_X \phi, \mathbf{a}_{0i}, \kappa) + \Psi_{\text{ext}}(\boldsymbol{\varphi}). \quad (4)$$

2.3 Total Potential Energy

The total potential energy of a system additively combines the internal contribution Π_{int} , reflecting the action of internal forces, and an external contribution $\Pi_{\text{ext}} = \Pi_{\text{vol}} + \Pi_{\text{sur}}$ due to volume and surface forces, i.e.

$$\Pi(\boldsymbol{\varphi}, \mathbf{F}, \phi, \nabla_X \phi; \mathbf{a}_{0i}, \kappa) = \Pi_{\text{int}} + \Pi_{\text{ext}}. \quad (5)$$

The internal energy contribution can be written as

$$\Pi_{\text{int}}(\mathbf{F}, \phi, \nabla_X \phi; \mathbf{a}_{0i}, \kappa) = \int_{\mathcal{B}_0} \Psi_{\text{int}} \, dV. \quad (6)$$

while the external contributions, assuming ‘dead’ loads, are provided by

$$\Pi_{\text{vol}}(\boldsymbol{\varphi}) = \int_{\mathcal{B}_0} \Psi_{\text{vol}} \, dV = - \int_{\mathcal{B}_0} \bar{\mathbf{B}} \cdot \boldsymbol{\varphi} \, dV, \quad (7)$$

$$\Pi_{\text{sur}}(\boldsymbol{\varphi}) = \int_{\partial \mathcal{B}_0} \Psi_{\text{sur}} \, dA = - \int_{\partial \mathcal{B}_0} \bar{\mathbf{T}} \cdot \boldsymbol{\varphi} \, dA, \quad (8)$$

where $\bar{\mathbf{B}}$ denotes the body force vector per unit reference volume and $\bar{\mathbf{T}}$ characterises the traction vector per unit reference surface area. In this regard, see, for instance, Waffenschmidt and Menzel [15] where a double-layered thick-walled cylindrical tube subjected to internal pressure is analysed on the basis of a total potential.

2.4 Variational Form

The boundary value problem is governed by the principle of minimum potential energy

$$\min_{\boldsymbol{\varphi}, \phi} \Pi(\boldsymbol{\varphi}, \mathbf{F}, \phi, \nabla_X \phi; \mathbf{a}_{0i}, \kappa), \quad (9)$$

which requires the first variation of the total potential energy with respect to $\boldsymbol{\varphi}$ and ϕ to vanish, i.e.

$$\delta_{\boldsymbol{\varphi}} \Pi(\boldsymbol{\varphi}, \mathbf{F}, \phi, \nabla_X \phi; \mathbf{a}_{0i}, \kappa) \doteq \mathbf{0} \quad \forall \quad \delta \boldsymbol{\varphi}, \quad (10)$$

$$\delta_{\phi} \Pi(\boldsymbol{\varphi}, \mathbf{F}, \phi, \nabla_X \phi; \mathbf{a}_{0i}, \kappa) \doteq 0 \quad \forall \quad \delta \phi. \quad (11)$$

Taking into account that $\delta_{\boldsymbol{\varphi}} W_{\text{int}} = \delta_{\boldsymbol{\varphi}} \Pi_{\text{int}}$ and $\delta_{\boldsymbol{\varphi}} W_{\text{ext}} = -\delta_{\boldsymbol{\varphi}} \Pi_{\text{ext}}$, we obtain a coupled system of variational equations, i.e.

$$\delta_{\boldsymbol{\varphi}} W = \delta_{\boldsymbol{\varphi}} W_{\text{int}} - \delta_{\boldsymbol{\varphi}} W_{\text{ext}} = \mathbf{0} \quad \forall \quad \delta \boldsymbol{\varphi}, \quad (12)$$

$$\delta_{\phi} W = \delta_{\phi} W_{\text{int}} - \delta_{\phi} W_{\text{ext}} = 0 \quad \forall \quad \delta \phi, \quad (13)$$

where the internal and external contributions are given in spatial form as

$$\delta_{\boldsymbol{\varphi}} W_{\text{int}} = \int_{\mathcal{B}_t} \boldsymbol{\sigma} : \nabla_{\mathbf{x}} \delta \boldsymbol{\varphi} \, d\mathbf{v}, \quad \delta_{\boldsymbol{\varphi}} W_{\text{ext}} = \int_{\mathcal{B}_t} \bar{\mathbf{b}} \cdot \delta \boldsymbol{\varphi} \, d\mathbf{v} + \int_{\partial \mathcal{B}_t} \bar{\mathbf{t}} \cdot \delta \boldsymbol{\varphi} \, d\mathbf{a}, \quad (14)$$

$$\delta_{\phi} W_{\text{int}} = \int_{\mathcal{B}_t} \mathbf{y} \cdot \nabla_{\mathbf{x}} \delta \phi \, d\mathbf{v}, \quad \delta_{\phi} W_{\text{ext}} = \int_{\mathcal{B}_t} y \delta \phi \, d\mathbf{v}. \quad (15)$$

Here the Cauchy stress $\boldsymbol{\sigma}$ and the vectorial damage quantity \mathbf{y} are related to *flux* terms, whereas the body force $\bar{\mathbf{b}}$ and the scalar damage quantity y are associated to *source* terms. They are defined as

$$\boldsymbol{\sigma} = \partial_{\mathbf{F}} \Psi \cdot \text{cof}(\mathbf{F}^{-1}), \quad \bar{\mathbf{b}} = -J^{-1} \partial_{\boldsymbol{\varphi}} \Psi_{\text{vol}}, \quad (16)$$

$$\mathbf{y} = \partial_{\nabla_X \phi} \Psi \cdot \text{cof}(\mathbf{F}^{-1}), \quad y = -J^{-1} \partial_{\phi} \Psi. \quad (17)$$

Relations (14) and (15) provide the basis for the finite element discretisation in Sect. 4.

3 Constitutive Relations

In this section, we first review the hyperelastic constitutive equations adopted on the basis of an isotropic neo-Hookean relation and an anisotropic exponential part. These relations characterise the *elastic* anisotropic response of the fibre-reinforced material. Secondly, we specify the gradient-enhanced, non-local contribution to the free energy, followed by the continuum damage formulation.

3.1 Hyperelastic Part of the Free Energy

From Sect. 2.2, we recall the local free energy density Ψ_{loc} , Eq. (1), to be additively composed of an isotropic part Ψ_{iso} , representing the isotropic matrix material, and

of an anisotropic part Ψ_{ani} , representing the individual families of fibres. In the following, we assume the isotropic part to be specified by a compressible neo-Hookean format

$$\Psi_{\text{iso}} = \frac{\mu_e}{2} [I_1 - 3] - \mu_e \ln(J) + \frac{\lambda_e}{2} [\ln(J)]^2, \quad (18)$$

with $I_1 = \mathbf{F} : \mathbf{F}$ denoting the first invariant. The elastic constants are represented by the Lamé-parameters μ_e and $\lambda_e = \kappa_e - 2/3 \mu_e$ in terms of the shear modulus μ_e and the bulk modulus κ_e . The anisotropic contribution of the local free energy (1) is based on an orthotropic exponential model with two families of fibres including fibre dispersion according to Gasser et al. [5] or Menzel et al. [12], i.e.

$$\Psi_{\text{ani}} = \frac{k_1}{2k_2} \sum_{i=1}^N \left[\exp \left(k_2 \langle E_i \rangle^2 \right) - 1 \right], \quad (19)$$

with the strain-like quantity $E_i = \varkappa I_1 + [1 - 3\varkappa] I_{4i} - 1$ and the invariant $I_{4i} = \mathbf{a}_{0i} \cdot \mathbf{F}^t \cdot \mathbf{F} \cdot \mathbf{a}_{0i}$ for $N = 2$ fibre families. The term $\langle E_i \rangle$, where $\langle \bullet \rangle = [|\bullet| + \bullet]/2$ is the Macaulay bracket, reflects the assumption that fibres can support tension only. Consequently, $\Psi_{\text{ani}} > 0$ only if the fibre-related strain is positive, i.e. $E_i > 0$. Fibre dispersion is introduced by means of the parameter $\varkappa \in [0, 1/3]$, where $\varkappa = 0$ corresponds to no dispersion, i.e. transverse isotropy, and where $\varkappa = 1/3$ renders an isotropic distribution. Table 1 summarises the structural and elastic material quantities included in constitutive Eqs. (18) and (19) together with their units. It is important to note that the fibre orientations may be defined arbitrarily, but the present formulation uses only *one* non-local damage variable so that both fibre families undergo identical degradation. This is physically meaningful as long as both families of fibers possess one and the same stretch history, otherwise a second non-local damage variable should be included in the formulation.

Table 1 Constitutive parameters as used in Sects. 3.1–3.3

Type	Symbol	Description	Unit
Structural	\mathbf{a}_{0i}	Fibre orientation vectors	–
	\varkappa	Dispersion parameter	–
Elastic	μ_e	Shear modulus	kPa
	κ_e	Bulk modulus	kPa
	k_1	Elastic constant	kPa
	k_2	Elastic constant	–
Regularisation	c_d	Degree of regularisation	kPa ⁻¹ mm ²
	β_d	Penalty parameter	kPa ⁻¹
Damage	η_d	Saturation parameter	kPa ⁻¹
	κ_d	Damage threshold	kPa

3.2 Gradient-Enhanced Part of the Free Energy

According to Eq. (2), we assume the non-local part of the free energy to be additively composed of a gradient-related term Ψ_{grd} and of a penalty term Ψ_{plty} and specify these terms as

$$\Psi_{\text{grd}}(\nabla_X \phi; \mathbf{F}) = \frac{c_d}{2} \|\nabla_X \phi\|^2 \quad \text{and} \quad \Psi_{\text{plty}}(\phi, \kappa) = \frac{\beta_d}{2} [\phi - \kappa]^2. \quad (20)$$

The energy-related penalty parameter β_d approximately enforces the local damage field κ and the non-local field ϕ to coincide. Furthermore, the gradient parameter c_d controls the quasi-non-local character of the formulation and characterises the degree of gradient regularisation: $c_d = 0$ results in a local model, while $c_d > 0$ leads to the regularised gradient-enhanced model. The damage-related parameters included in constitutive Eq. (20) together with their units are summarised in Table 1.

3.3 Gradient-Enhanced Damage Model

In order to obtain the stress-like thermodynamic forces driving the local dissipative damage process, we follow the standard Coleman-Noll procedure. Differentiation of the general format of the free energy (3) with respect to time and application of the Clausius-Planck inequality yields, amongst others, a contribution including the thermodynamic force $q = q_{\text{loc}} + q_{\text{nloc}} = -\partial_d \Psi$ conjugate to the damage variable d , i.e.

$$q_{\text{loc}} = \Psi_{\text{ani}} \quad \text{and} \quad q_{\text{nloc}} = \beta_d [\phi - \kappa] \partial_d \kappa. \quad (21)$$

Furthermore, we adopt the damage condition

$$\Phi_d = q - \kappa \leq 0 \quad (22)$$

where $\Phi_d < 0$ refers to the purely elastic loading and $\Phi_d = 0$ to damage evolution. Based on the postulate of maximum dissipation, we construct a constrained optimisation problem involving the Lagrange multiplier λ . This results in the following associated evolution equation for the damage variable

$$\dot{\kappa} = \lambda \frac{\partial \Phi_d}{\partial q} = \lambda \quad \text{with} \quad \kappa|_{t=0} = \kappa_d. \quad (23)$$

where initiation and termination of damage are governed by the Karush-Kuhn-Tucker complementary conditions

$$\lambda \geq 0, \quad \Phi_d \leq 0, \quad \lambda \Phi_d = 0. \quad (24)$$

We assume an exponential behaviour for the damage function

$$f_d(\kappa) = 1 - d = \exp(\eta_d [\kappa_d - \kappa]), \quad (25)$$

with $\eta_d > 0$ so that $\partial_d \kappa = [\eta_d f_d(\kappa)]^{-1} > 0$ and introduce an initial damage threshold κ_d , which must be exceeded in order to activate damage evolution. Furthermore, we include a saturation parameter η_d . It becomes apparent that larger values of η_d accelerate the damage process, whereas larger values of κ_d lead to a delay of the damage initiation. Note, that for the limiting case $\kappa_d = 0$, damage is initiated from the very beginning of the loading process, whereas damage does not evolve for $\kappa_d \rightarrow \infty$.

4 Finite Element Discretisation

This section deals with the spatial finite element discretisation of the underlying coupled system of non-linear equations. This includes a combination of tri-quadratic serendipity interpolation functions with respect to the displacement field, and tri-linear interpolation functions with respect to the non-local damage field variable where we outline an efficient and compact FE-implementation using a common Voigt-notation-based vector-matrix-format.

4.1 Discretisation

We discretise the domain \mathcal{B}_0 by n_{el} finite elements, so that $\mathcal{B}_0 \approx \mathcal{B}_0^h = \bigcup_{e=1}^{n_{\text{el}}} \mathcal{B}_{0e}$, where every finite element \mathcal{B}_{0e} is characterised by n_{en}^φ placement-nodes and n_{en}^ϕ non-local-damage-nodes. According to the isoparametric concept, we interpolate the field variables $\boldsymbol{\varphi}$ as well as the geometry \mathbf{X} by the same shape functions N^φ

$$\mathbf{X} \approx \mathbf{X}^h = N^\varphi \cdot \mathbf{X}_e, \quad \boldsymbol{\varphi} \approx \boldsymbol{\varphi}^h = N^\varphi \cdot \boldsymbol{\varphi}_e, \quad (26)$$

and transform them to a hexahedral reference element with natural coordinates $\boldsymbol{\xi} := \{\xi, \eta, \zeta\} \in \tilde{\mathcal{B}}$, where $\tilde{\mathcal{B}} := \{\boldsymbol{\xi} \in \mathbb{R}^3 \mid -1 \leq \chi \leq +1; \chi = \xi, \eta, \zeta\}$ denotes the reference domain. In the present context, the number of displacement-nodes and non-local-damage-nodes per element—and consequently the related shape functions—do not necessarily have to coincide, i.e. $n_{\text{en}}^\varphi \neq n_{\text{en}}^\phi$ and $N^\varphi \neq N^\phi$. We approximate the associated field variables, i.e. the placement $\boldsymbol{\varphi}$ and the non-local damage variable ϕ by means of the product of shape functions $N^\alpha(\boldsymbol{\xi})$, $\alpha = \varphi, \phi$ and discrete element degrees of freedom $\boldsymbol{\varphi}_e$ and ϕ_e , i.e.

$$\boldsymbol{\varphi}^h = N^\varphi \cdot \boldsymbol{\varphi}_e, \quad \phi^h = N^\phi \cdot \phi_e, \quad (27)$$

and introduce the shape functions in matrix form as

$$\mathbf{N}^\varphi = \begin{bmatrix} N_1^\varphi & 0 & 0 & \dots & N_{n_{\text{en}}}^\varphi & 0 & 0 \\ 0 & N_1^\varphi & 0 & \dots & 0 & N_{n_{\text{en}}}^\varphi & 0 \\ 0 & 0 & N_1^\varphi & \dots & 0 & 0 & N_{n_{\text{en}}}^\varphi \end{bmatrix}, \quad \mathbf{N}^\phi = \begin{bmatrix} N_1^\phi & \dots & N_{n_{\text{en}}}^\phi \end{bmatrix}. \quad (28)$$

Similarly, the spatial gradients $\nabla_{\mathbf{x}}\boldsymbol{\varphi}$ and $\nabla_{\mathbf{x}}\phi$ of the placement $\boldsymbol{\varphi}$ and the non-local damage variable ϕ are approximated by means of

$$\nabla_{\mathbf{x}}\boldsymbol{\varphi}^{\text{h}} = \mathbf{B}^\varphi \cdot \boldsymbol{\varphi}_e, \quad \nabla_{\mathbf{x}}\phi^{\text{h}} = \mathbf{B}^\phi \cdot \phi_e, \quad (29)$$

where we express the spatial gradients of the shape functions $N_{n_{\text{en}},x}^\alpha := \nabla_{\mathbf{x}} N_{n_{\text{en}}}^\alpha$ in matrix form as

$$\mathbf{B}^\varphi = \begin{bmatrix} N_{1,x}^\varphi & 0 & 0 & \dots & N_{n_{\text{en}},x}^\varphi & 0 & 0 \\ 0 & N_{1,y}^\varphi & 0 & \dots & 0 & N_{n_{\text{en}},y}^\varphi & 0 \\ 0 & 0 & N_{1,z}^\varphi & \dots & 0 & 0 & N_{n_{\text{en}},z}^\varphi \\ N_{1,y}^\varphi & N_{1,x}^\varphi & 0 & \dots & N_{n_{\text{en}},y}^\varphi & N_{n_{\text{en}},x}^\varphi & 0 \\ N_{1,z}^\varphi & 0 & N_{1,x}^\varphi & \dots & N_{n_{\text{en}},z}^\varphi & 0 & N_{n_{\text{en}},x}^\varphi \\ 0 & N_{1,z}^\varphi & N_{1,y}^\varphi & \dots & 0 & N_{n_{\text{en}},z}^\varphi & N_{n_{\text{en}},y}^\varphi \end{bmatrix}, \quad \mathbf{B}^\phi = \begin{bmatrix} N_{1,x}^\phi & \dots & N_{n_{\text{en}},x}^\phi \\ N_{1,y}^\phi & \dots & N_{n_{\text{en}},y}^\phi \\ N_{1,z}^\phi & \dots & N_{n_{\text{en}},z}^\phi \end{bmatrix}. \quad (30)$$

According to the Bubnov-Galerkin method, we apply an analogous approximation for the variations of field variables and corresponding gradients. The discretised weak form on element level is characterised by the difference of the element-specific internal and external virtual work related terms $\delta_\varphi W_{e \text{ int}}$ and $\delta_\varphi W_{e \text{ ext}}$, so that

$$\delta_\varphi W_e = \delta_\varphi W_{e \text{ int}} - \delta_\varphi W_{e \text{ ext}} = \mathbf{0} \quad \forall \quad \delta \boldsymbol{\varphi}_e, \quad (31)$$

$$\delta_\phi W_e = \delta_\phi W_{e \text{ int}} - \delta_\phi W_{e \text{ ext}} = \mathbf{0} \quad \forall \quad \delta \phi_e, \quad (32)$$

where the discrete representations take the following forms

$$\delta_\varphi W_{e \text{ int}} = \delta \boldsymbol{\varphi}_e \cdot \mathbf{f}_{e \text{ int}}^\varphi \quad \text{with} \quad \mathbf{f}_{e \text{ int}}^\varphi = \int_{\mathcal{B}_t} \mathbf{B}^{\varphi^{\text{t}}} \cdot \boldsymbol{\sigma}^{\text{v}} \, \text{d}v, \quad (33)$$

$$\delta_\varphi W_{e \text{ ext}} = \delta \boldsymbol{\varphi}_e \cdot \mathbf{f}_{e \text{ ext}}^\varphi \quad \text{with} \quad \mathbf{f}_{e \text{ ext}}^\varphi = \int_{\mathcal{B}_t} N^{\varphi^{\text{t}}} \cdot \bar{\mathbf{b}} \, \text{d}v + \int_{\partial \mathcal{B}_t} N^{\varphi^{\text{t}}} \cdot \bar{\mathbf{t}} \, \text{d}a, \quad (34)$$

$$\delta_\phi W_{e \text{ int}} = \delta \phi_e \cdot \mathbf{f}_{e \text{ int}}^\phi \quad \text{with} \quad \mathbf{f}_{e \text{ int}}^\phi = \int_{\mathcal{B}_t} \mathbf{B}^{\phi^{\text{t}}} \cdot \mathbf{y} \, \text{d}v, \quad (35)$$

$$\delta_\phi W_{e \text{ ext}} = \delta \phi_e \cdot \mathbf{f}_{e \text{ ext}}^\phi \quad \text{with} \quad \mathbf{f}_{e \text{ ext}}^\phi = \int_{\mathcal{B}_t} N^{\phi^{\text{t}}} \, \text{d}v, \quad (36)$$

and Voigt-notation is denoted by the superscript v . Applying the fundamental lemma of calculus of variations, this results in the residual form of the present coupled problem

$$\mathbf{r}_e^\varphi = \mathbf{f}_{e \text{ int}}^\varphi - \mathbf{f}_{e \text{ ext}}^\varphi = \mathbf{0}, \quad (37)$$

$$\mathbf{r}_e^\phi = \mathbf{f}_{e \text{ int}}^\phi - \mathbf{f}_{e \text{ ext}}^\phi = \mathbf{0}. \quad (38)$$

4.2 Linearisation

The governing system of Eqs. (37) and (38) is coupled with respect to the motion φ and the non-local damage field ϕ , which itself is linked to the local damage variable κ by means of the penalty term. To solve this highly non-linear system of equations, we use an incremental-iterative Newton-Raphson scheme where we subsequently omit the subscript index $n + 1$ associated with time t_{n+1} for the sake of readability. A Taylor series expansion around the solution at the current iteration step k up to the linear term gives

$$\mathbf{r}_{e k+1}^\varphi = \mathbf{r}_{e k}^\varphi + \frac{d\mathbf{r}_e^\varphi}{d\varphi} \cdot \Delta\varphi + \frac{d\mathbf{r}_e^\varphi}{d\phi} \cdot \Delta\phi = \mathbf{0}, \quad (39)$$

$$\mathbf{r}_{e k+1}^\phi = \mathbf{r}_{e k}^\phi + \frac{d\mathbf{r}_e^\phi}{d\varphi} \cdot \Delta\varphi + \frac{d\mathbf{r}_e^\phi}{d\phi} \cdot \Delta\phi = \mathbf{0}. \quad (40)$$

Herein, the increments $\Delta\varphi = \varphi_{k+1} - \varphi_k$ and $\Delta\phi = \phi_{k+1} - \phi_k$ represent the difference of the discrete nodal degrees of freedom at iteration-step $k + 1$ and k . Assuming ‘dead loads’, we deduce the element-specific sub-matrices of the Jacobian as

$$\mathbf{K}_e^{\varphi\varphi} = \frac{d\mathbf{r}_e^\varphi}{d\varphi} = \int_{\mathcal{B}_i^e} \left[\mathbf{B}^{\varphi^t} \cdot \mathbf{e}^v \cdot \mathbf{B}^\varphi + [\mathbf{G}^\varphi \cdot \boldsymbol{\sigma} \cdot \mathbf{G}^{\varphi^t}] \odot \mathbf{I} \right] dv, \quad (41)$$

$$\mathbf{K}_e^{\varphi\phi} = \frac{d\mathbf{r}_e^\varphi}{d\phi} = \int_{\mathcal{B}_i^e} \mathbf{B}^{\varphi^t} \cdot \left[\frac{d\boldsymbol{\sigma}}{d\phi} \right]^v \cdot \mathbf{N}^\phi dv, \quad (42)$$

$$\mathbf{K}_e^{\phi\varphi} = \frac{d\mathbf{r}_e^\phi}{d\varphi} = \int_{\mathcal{B}_i^e} \mathbf{N}^{\phi^t} \cdot \left[2 \frac{dy}{dg} \right]^v \cdot \mathbf{B}^\varphi dv, \quad (43)$$

$$\mathbf{K}_e^{\phi\phi} = \frac{d\mathbf{r}_e^\phi}{d\phi} = \int_{\mathcal{B}_i^e} \left[\mathbf{N}^{\phi^t} \cdot \left[\frac{dy}{d\phi} \right]^v \cdot \mathbf{N}^\phi + \mathbf{B}^{\phi^t} \cdot \left[\frac{dy}{d\nabla_x \phi} \right]^v \cdot \mathbf{B}^\phi \right] dv, \quad (44)$$

allowing us to express the geometrical contribution of $\mathbf{K}^{\varphi\varphi}$ conveniently by means of the Kronecker product \odot . Furthermore, \mathbf{e} , $d\boldsymbol{\sigma}/d\phi$, $2 dy/dg$, $dy/d\phi$ and $dy/d\nabla_x \phi$

denote partitions of the consistent tangent-moduli as specified in Waffenschmidt et al. [16]. This results in the following symmetric linearised system of equations

$$\begin{bmatrix} \mathbf{r}_e^\varphi \\ \mathbf{r}_e^\phi \end{bmatrix} + \begin{bmatrix} \mathbf{K}_e^{\varphi\varphi} & \mathbf{K}_e^{\varphi\phi} \\ \mathbf{K}_e^{\phi\varphi} & \mathbf{K}_e^{\phi\phi} \end{bmatrix} \cdot \begin{bmatrix} \Delta\boldsymbol{\varphi}_e \\ \Delta\boldsymbol{\phi}_e \end{bmatrix} = \begin{bmatrix} \mathbf{0} \\ \mathbf{0} \end{bmatrix} \quad (45)$$

for the determination of the unknown increments of the element degrees of freedom $\Delta\boldsymbol{\varphi}_e$ and $\Delta\boldsymbol{\phi}_e$. The assembly of all elements results in the global linearised system of equations in the k th iteration step

$$\mathbf{r} + \mathbf{K} \cdot \Delta\mathbf{d} = \mathbf{0} \quad \text{with} \quad \Delta\mathbf{d} = \mathbf{d}_{k+1} - \mathbf{d}_k, \quad (46)$$

with \mathbf{K} being the global tangent stiffness matrix, $\Delta\mathbf{d}$ the global incremental vector of degrees of freedom, \mathbf{r} the global residual vector including the internal and external system loads.

5 Residual Stresses

The incorporation of residual stresses is of key importance within the modelling and simulation of soft biological tissues. Different concepts have been discussed in the literature to account for these equilibrated stress contributions present in the absence of external loading. The procedure employed here to incorporate such effects is based on a multiplicative composition of the total deformation gradient as discussed by Johnson and Hoger [7] and Holzapfel et al. [6]. To be specific, we consider a stress-free reference configuration \mathcal{B}_0 , a load-free residually stressed configuration \mathcal{B}_{res} and a current configuration \mathcal{B}_t , cf. Fig. 1. In this regard, we—on the one hand—introduce a deformation gradient-type tensor \mathbf{F}_{res} which transforms line elements from the stress-free reference configuration \mathcal{B}_0 to the residually stressed configuration \mathcal{B}_{res} and—on the other hand—another deformation gradient-type tensor \mathbf{F}_p which transforms line elements from the residually stressed configuration \mathcal{B}_{res} to the current configuration \mathcal{B}_t . The resulting deformation gradient tensor can then be written in terms of cylindrical base vectors as

$$\mathbf{F} = \mathbf{F}_p \cdot \mathbf{F}_{\text{res}} = \lambda_i \mathbf{e}_i \otimes \mathbf{E}_i \mid_{i \in \{r, \theta, z\}}. \quad (47)$$

For a perfect cylindrical geometry, the radial and the circumferential principal stretches can be expressed in terms of spatial cylindrical coordinates $\{r, \theta, z\}$ as $\lambda_r = R/[r k \lambda_z]$ and $\lambda_\theta = r k/R$, where $R = \sqrt{k \lambda_z [r^2 - r_i^2] + R_i^2}$. In these relations, we prescribe the inner radius of the closed configuration r_i , the inner radius of the opened configuration R_i , the opening angle α , and the axial residual stretch λ_z , and introduce the opening angle parameter as $k = 2\pi/[2\pi - \alpha]$. Composition (47) can

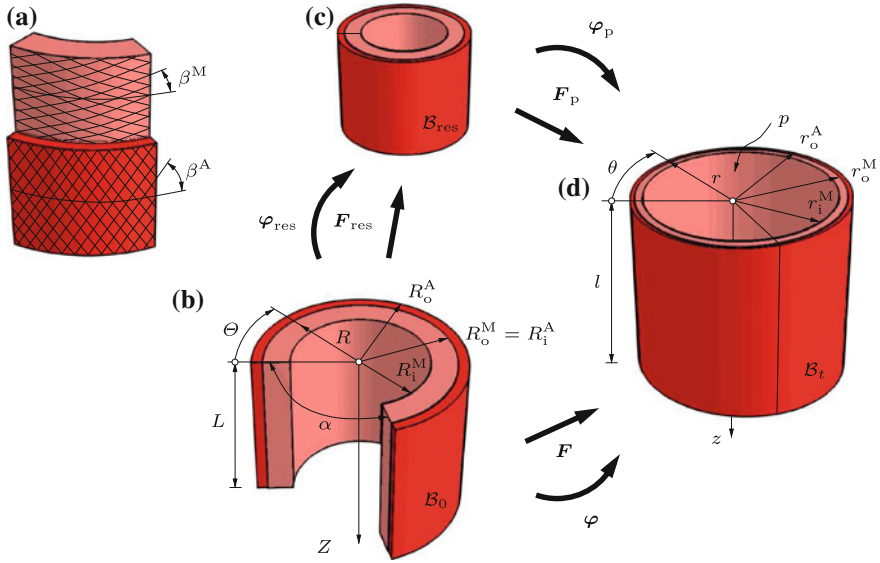


Fig. 1 Deformation modes of a double-layered thick-walled cylindrical tube, cf. Holzapfel et al. [6]: bending (opening angle α), inflation (internal pressure p), and extension (axial stretch λ_z); **a** segment of the arterial wall consisting of media (M) and adventitia (A) reinforced by two families of fibres with fibre angles β^M, β^A defined in **b** a stress-free reference configuration \mathcal{B}_0 ; **c** residually stressed but load-free configuration \mathcal{B}_{res} ; **d** residually stressed and loaded current configuration \mathcal{B}_t . (Adopted from Waffenschmidt and Menzel [15] with kind permission of Elsevier.)

conveniently be used to model residual stresses within finite element formulations for the simulation of tube-like boundary value problems; see Sect. 6.1.

6 Numerical Examples

In order to highlight the mechanical modelling capabilities as well as the computational performance of the presented model, we discuss some illustrative three-dimensional finite element examples. To be specific, we study the degradation of a fibre-reinforced artery-like tube subjected to internal pressure. As a crucial aspect of this contribution, residual stresses are incorporated by means of the technique described in Sect. 5.

6.1 Reproduction of the Opening Angle Experiment

Residual circumferential stresses can be revealed by the *opening angle experiment*, where a short ring of an artery is cut in radial direction. The residual stresses through

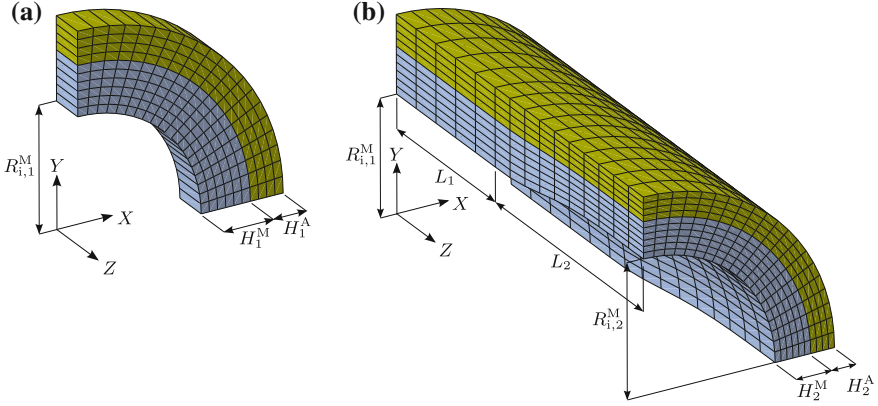


Fig. 2 Geometry and finite element mesh of the thick-walled double-layered tube, where only one quarter is shown. **a** Perfect tube. **b** Perturbed tube

the artery cause the ring to spring open to form an open sector. We now carry out a numerical reproduction of the opening angle experiment for a thick-walled double-layered tube, in order to assess whether the method provided in Sect. 5 yields accurate results. This technique allows for the inclusion of different opening angles for the different arterial layers within only one simulation. For this purpose, it is necessary to create an initial deformation gradient \mathbf{F}_{res} at each Gauss-point of a related finite element mesh. Note that \mathbf{F}_{res} must be inhomogeneously distributed as also the residual stresses are. This deformation gradient field has to be provided in terms of the underlying coordinate system used by the finite element code which is typically described by a Cartesian basis. The procedure to calculate the initial residual strain field by means of the deformation gradient tensor \mathbf{F}_{res} is described in detail in, for instance, Waffenschmidt [14].

The geometrical setting essentially reflects the geometry of a healthy coronary artery. We use two different geometries, i.e. (i) a perfect tube with constant thickness and (ii) a perturbed tube with variable thickness, see Fig. 2. The perturbed tube is represented by two different cross-sections. A first cross-section (length L_1) with constant inner radius $R_{i,1}^M$ and a second cross-section with different inner radii $R_{i,1}^M$ and $R_{i,2}^M$. The outer radius R_o remains constant over the whole length. The functional relation of R_i^M for $Z \in [L_1, L_2]$ is provided by

$$R_i^M(\bar{Z}) = -0.904 \bar{Z}^5 + 3.913 \bar{Z}^4 - 5.756 \bar{Z}^3 + 3.259 \bar{Z}^2 - 0.317 \bar{Z} + 0.006, \quad (48)$$

where $\bar{Z} = [Z - L_1]/L_2$ such that $R_i^M(Z = L_1) = R_{i,1}^M$ and $R_i^M(Z = L_1 + L_2) = R_{i,2}^M$. The geometrical, structural and material parameters for both geometries are summarised in Table 2. We choose four different sets of the opening angles α^n , whereas we neglect the influence of the axial residual stretch at this stage, i.e. $\lambda_z = 1.0$. The initial orientations of the fibres are assumed as $\mathbf{a}_{0,1,2}^n = \sin(\beta^n) \mathbf{e}_Z \pm$

Table 2 Set of parameters as used in the numerical examples ($n = M$ for the media and $n = A$ for the adventitia)

Type	Symbol	Value		Unit
		Media	Adventitia	
Geometrical	$R_{i,1}^n$	1.35	1.89	mm
	H_1^n	0.54	0.36	mm
	$R_{i,2}^n$	1.55	1.97	mm
	H_2^n	0.42	0.28	mm
	L_1	2.0		mm
	L_2	3.0		mm
Structural	β^n	21.700	62.260	deg
	ε^n	0.19	0.036	–
	α^n	{0.0, 45.0, 60.0, 120.0}	{0.0, 90.0, 120.0, 160.0}	deg
Elastic	μ_c^n	27.0	2.7	kPa
	κ_c^n	2700.0	270.0	kPa
	k_1^n	0.64	5.1	kPa
	k_2^n	7.08	30.8	–
Regularisation	c_d	{0.08, 0.5, 3.0}		$\text{kPa}^{-1}\text{mm}^2$
	β_d	1000.0		kPa^{-1}
Damage	η_d	0.25		kPa^{-1}
	κ_d	5.0		kPa

$\cos(\beta^n) \mathbf{e}_\Theta$ with $n = M$ for the media and $n = A$ for the adventitia. The perfect tube is discretised by 800, the perturbed tube by 12,000 finite elements. Since we prescribe the radii R_i^n of the opened configuration and the opening angles α^n as input parameters to create the residual strain field, we expect to reproduce these values at least approximately as well as a complete stress release at the end of the simulation. Basically the FE-simulation of the opening angle experiment is subdivided into a sequence of two calculation steps:

1. *Application of the residual strain field* at Gauss-point-level: apply homogeneous Dirichlet boundary conditions at all nodes in circumferential and axial direction.
2. *Radial cut*: apply homogeneous Dirichlet boundary conditions at two nodes in radial direction, at all nodes located at the cut in circumferential direction and at all nodes at back face in axial direction.

In this regard, all boundary conditions are removed from one step to another and re-specified for those boundary conditions that are to be retained. If a boundary condition is removed, it will be replaced by a concentrated force equal to the reaction force calculated at the restrained degree of freedom at the end of the previous step. This concentrated force will then be linearly reduced to zero over the period of the step. In this case, both layers are separated from each other in order to give an illustrative view

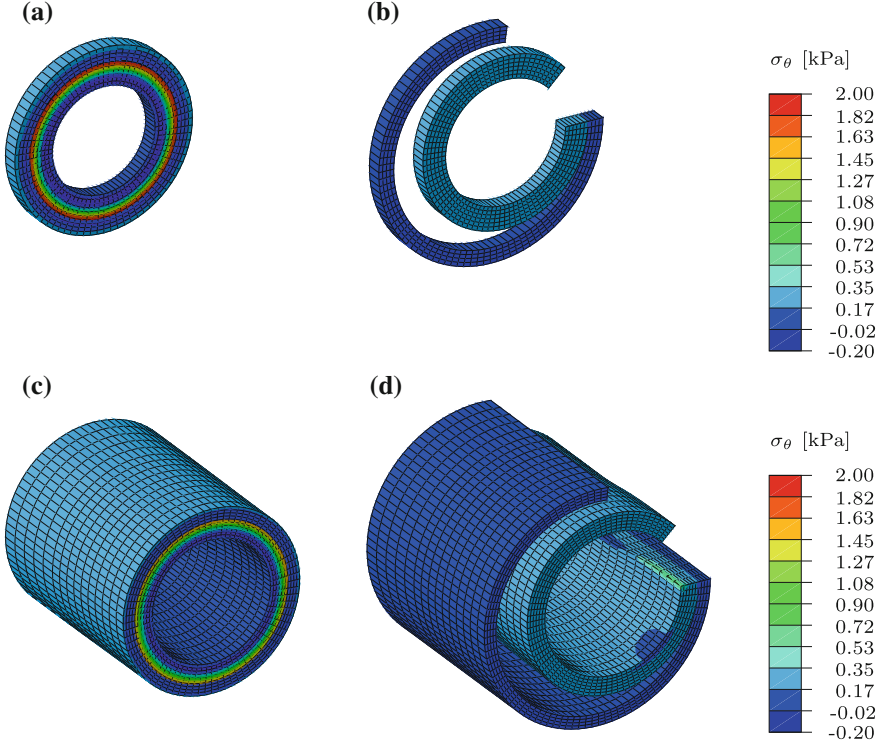


Fig. 3 Reproduction of the opening angle experiment with prescribed opening angles $\alpha^M = 45.0$ [deg], $\alpha^A = 90.0$ [deg]. Circumferential Cauchy stress σ_θ after **a** the application of the residual strain field, **b** the radial cut

of the effect of different prescribed opening angles and radii which, for the purpose of illustration, are set to values of $R_i^M = 1.5$ [mm], $R_i^A = 2.5$ [mm], $\alpha^M = 45.0$ [deg] and $\alpha^A = 90.0$ [deg]. As a consequence of the initial imposition of the residual strain field, we obtain a stretching and warping of the cross-section of the tube. As both layers are separated from each other, this consequently results in an undesired penetration. In order to avoid this, a contact condition is prescribed between outer media and inner adventitia in the first simulation step.

Figure 3 illustrates the contours of the circumferential Cauchy stress σ_θ at different configurations \mathcal{B}_0 and \mathcal{B}_{res} of the simulation for the perfect tube (Fig. 3a, b) and the perturbed tube (Fig. 3c, d). It becomes apparent that the technique described above is able to appropriately reproduce the prescribed input parameters, so that $R_{i\text{sim}}^M \approx R_i^M$, $R_{i\text{sim}}^A \approx R_i^A$, $\alpha_{\text{sim}}^M \approx \alpha^M$ and $\alpha_{\text{sim}}^A \approx \alpha^A$ and $\sigma_\theta \approx 0$. Furthermore, the stress levels approximately agree for both cases. This underlines that the assumption of a perfect cylindrical tube is—in this case—a valid approximation for residual stress imposition of a slightly perturbed tube as used in this contribution.

6.2 Inflation of the Perturbed Tube

We continue with a study of the pressure-driven inflation problem of the perturbed tube. First, we focus on the elastic response and the effect of the residual stresses on the overall behaviour of the structure. Due to the symmetry of the inflation problem, it is sufficient to consider only one quarter of the perturbed tube resulting in 3,000 finite elements, as shown in Fig. 2.

6.2.1 Elastic Response

Figure 4a shows the load-displacement diagram in terms of the internal pressure p over the radial displacement $u_{r,i}$ at the inner radius of the tube at $z = L_1 + L_2$. Two different elastic solutions are shown: the isotropic neo-Hookean matrix in the lower dotted curves, and the overall elastic response composed of the neo-Hookean matrix *and* the fibre reinforced material in the upper solid curves. These curves give a good illustration of the highly non-linear material behaviour especially at large strains. As a consequence of the residual stresses, we basically obtain two significant effects. First, we observe a shift towards negative radial displacements. Secondly, we observe a shift towards higher pressure values. Both effects are directly related to the contraction of the tube due to the residual stresses. The contraction basically implies a change in the configuration in which the pressure is applied, i.e. for a reduced inner radius a larger pressure must be applied in order to obtain the same radial displacement. This is qualitatively in line with the solution for thick-walled cylinders under internal pressure in linear elasticity.

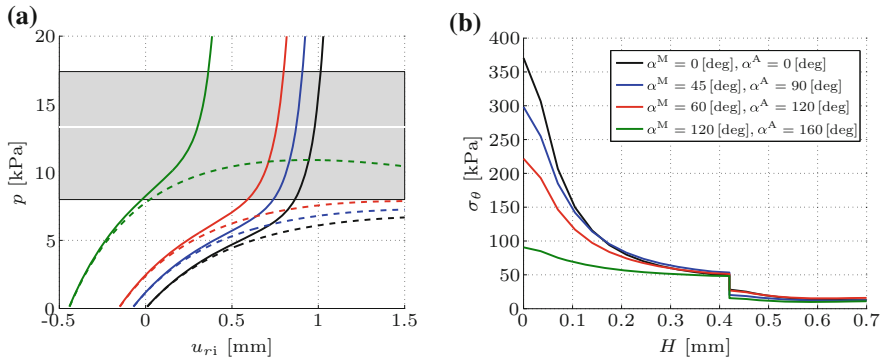


Fig. 4 Perturbed tube subjected to internal pressure and residual stresses. Variation of different sets of opening angles α^n . *Solid lines* represent the response of the fibre-reinforced material, *dotted lines* represent the response of the neo-Hookean matrix at $z = L_1 + L_2$. **a** Pressure p versus inner radial displacement $u_{r,i}$, where the *grey region* represents the physiological pressure range; **b** distribution of the circumferential Cauchy stress σ_θ along the undeformed thickness H at $p = 13.33$ [kPa]

The residual stresses also affect the distribution of the circumferential stresses over the undeformed tube thickness H , see Fig. 4b for a physiological (mean) internal pressure of $p = 13.33$ [kPa]. Apart from the discontinuity in the stress distribution which is due to the different material properties in media and adventitia, we observe that the stresses are significantly homogenised over the tube thickness and that their maximum value is dramatically reduced. This effect has a direct impact on the characteristic pressure range in which inelastic damage processes start to evolve as a result of high strain energy and stress levels. This effect is studied in more detail in the subsequent section.

6.2.2 Inelastic Response

Next, we study the degradation of the fibre-reinforced perturbed tube. As we are dealing with a force-driven boundary value problem, we use an arc-length method in order to trace the equilibrium path in case of snap-back-related instabilities. A maximum inner radial displacement of $u_{r,i} = 1.5$ [mm] is set as a limiting point in the load-displacement diagram shown in Fig. 5. Furthermore, we choose an appropriate set of material parameters to initiate the damage process as soon as the pressure exceeds the systolic blood pressure of approximately $p \approx 20.0$ [kPa]. The results are indicated in Fig. 5, where we adjust the pressure plot-range to a maximum value of 70.0 [kPa]. As a consequence, the stiffening due to the residual-stress-induced contraction is no longer visible but still present. The lower solid black curve represents the elastic response of the neo-hookean ground substance, the upper solid black curve represents the elastic response of the fibre-reinforcement material. The colored lines represent the response of the damaging structure. As only the fibres are assumed to be affected by the damage, the associated response is always located between these two black lines representing the elastic response. Upon successive damage of the fibres, the structural response converges to the response of the undamaged neo-Hookean matrix. The curves associated to $c_d = \{0.5, 3.0\}$ [kPa⁻¹ mm²] in Fig. 5a–c show a characteristic snap-back behaviour and follow the neo-Hookean unloading path once the fibres are completely damaged. As an interesting effect, the incorporation of residual stresses leads to an increase of the peak pressure before the overall structural response enters the unloading path. This is a direct consequence of the homogenisation-tendency of the circumferential stresses: as observed in Fig. 4b, larger opening angles α^n entail a larger reduction in the maximum circumferential stress σ_θ . Therefore, higher pressure levels can be sustained before the strain energy reaches the threshold to initiate the damage evolution. Particularly Fig. 5d shows that the structure exhibits almost no degradation for $c_d = \{0.5, 3.0\}$ [kPa⁻¹ mm²].

Furthermore, we investigate the effect of the regularisation parameter c_d . Generally, smoother distributions for the non-local damage variable ϕ and the damage function f_d are obtained for larger values of c_d . This is illustrated in Fig. 6, where the damage function f_d is shown for $\alpha^M = 45.0$ [deg], $\alpha^A = 90.0$ [deg] and different values of c_d at a post-peak pressure of $p = 40.0$ [kPa], i.e. a point within the unloading

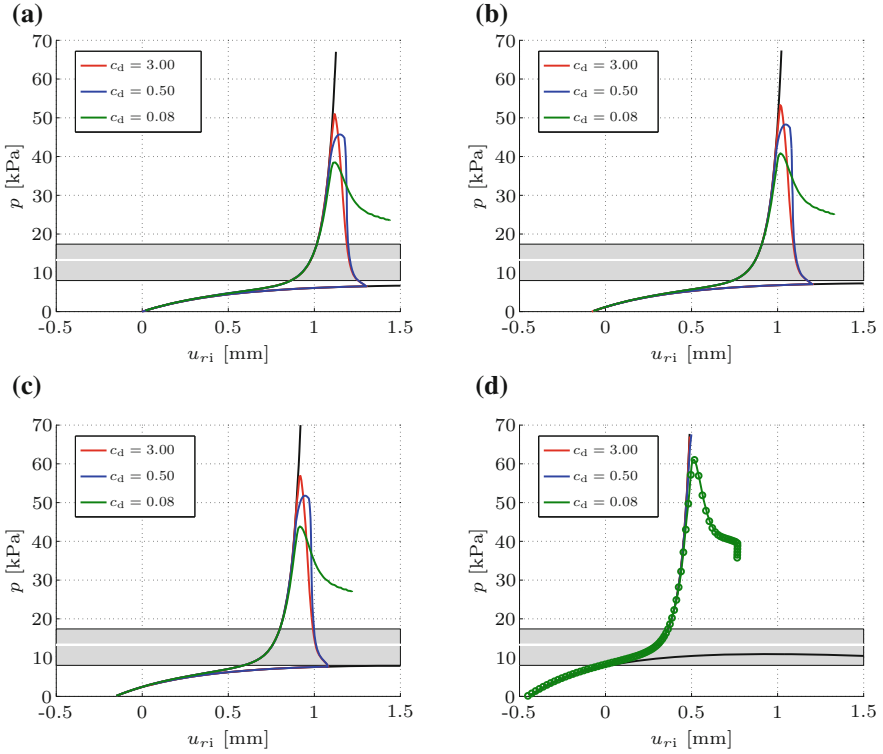


Fig. 5 Perturbed tube subjected to internal pressure and residual stresses. Variation of the regularisation parameter c_d in $[\text{kPa}^{-1} \text{mm}^2]$ for different sets of opening angles α^n . The *upper* and *lower solid black lines* represent the purely elastic response of the fibre-reinforced material and the neo-Hookean matrix. The *colored lines* represent the damage response. **a** $\alpha^M = 0.0$, $\alpha^A = 0.0$, **b** $\alpha^M = 45.0$, $\alpha^A = 90.0$, **c** $\alpha^M = 60.0$, $\alpha^A = 120.0$, **d** $\alpha^M = 120.0$, $\alpha^A = 160.0$ where the *circular markers* are associated with a mesh of 12,000 elements. The *grey region* represents the physiological pressure range. Units of α^n in [deg]

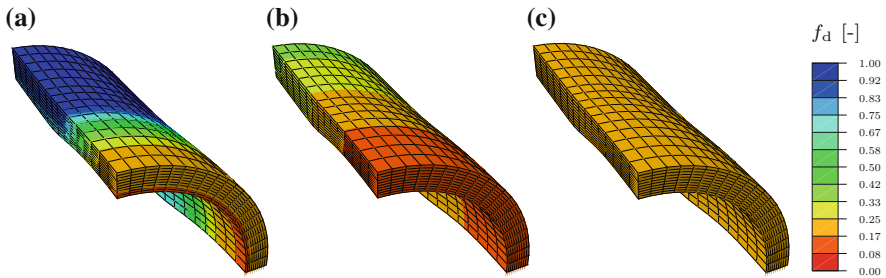


Fig. 6 Perturbed tube subjected to internal pressure and residual stresses. Contours of the damage function f_d for $\alpha^M = 45.0$ [deg], $\alpha^A = 90.0$ [deg] at a post-peak pressure of $p = 40.0$ [kPa]. Variation of f_d with **a** $c_d = 0.08$, **b** $c_d = 0.5$, **c** $c_d = 3.0$. Units of c_d in $[\text{kPa}^{-1} \text{mm}^2]$

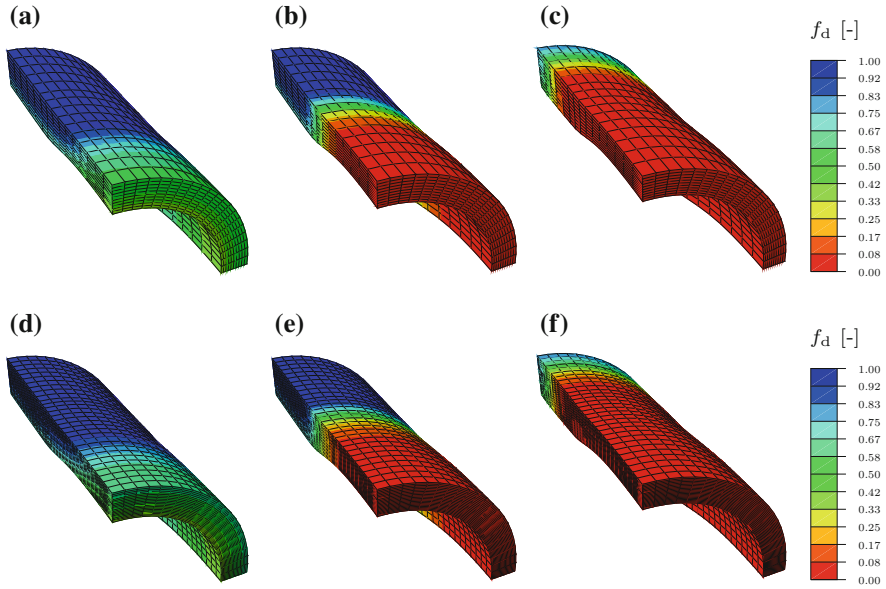


Fig. 7 Perturbed tube subjected to internal pressure and residual stresses. Contour plots of f_d with $\alpha^M = 120.0$ [deg], $\alpha^A = 160.0$ [deg], and $c_d = 0.08$ [kPa $^{-1}$ mm 2]. Successive snapshots along the unloading path at pressure levels $p = \{61.08, 42.89, 36.33\}$ [kPa]. (a–c) associated with 3,000 elements; (d–f) associated with 12,000 elements

path. It becomes apparent that smaller values of c_d cause the damage distribution to be more localised towards the thinner portion of the tube.

Finally, Fig. 7 shows the evolution of the damage function f_d for the prestressed tube for $\alpha^M = 120.0$ [deg], $\alpha^A = 160.0$ [deg] and $c_d = 0.08$ [kPa $^{-1}$ mm 2]. Three successive snapshots along the unloading path are shown in Fig. 7a–d which correspond to pressure levels of $p = \{61.08, 42.89, 36.33\}$ [kPa] for a discretisation of 3,000 elements. We observe that damage is first initiated at the thinnest section of the tube and later on evolves across the structure. Figure 7d–f show the same quantities for a finer discretisation of 12,000 elements. No substantial differences between both discretisations can be observed. Moreover Fig. 5d shows the load-displacement curves for both discretisations and again both curves almost completely coincide. This underlines the mesh-objective properties of the present gradient-enhanced damage model.

7 Summary

A well-known problem related to *local* continuum damage formulations is the possible ill-posedness of the underlying boundary value problem. As a consequence, finite element simulation results turn out to significantly depend on the discretisation. Typically, this is indicated by a vanishing localised damage zone, which is constrained only by the mesh resolution.

One possibility to regularise the problem, is the use of non-local continuum formulations. In this contribution, we present a non-local gradient-enhanced damage model within a finite strain setting. We implicitly regularise the problem by enhancing the local free energy with the gradient of the non-local damage variable and ensure the equivalence between the local and non-local damage field variable by a penalisation term incorporated within the free energy. The local elastic constitutive response is represented by a hyperelastic format, additively composed of an isotropic and an anisotropic part. The inelastic response is governed by a scalar $[1-d]$ -damage approach, affecting the anisotropic elastic part only. As another major aspect of this contribution, we incorporate residual stresses which are crucial for the modelling of soft biological tissues such as arteries. The procedure employed here to incorporate these effects is based on a multiplicative composition of the total deformation gradient.

We present a biomechanics-related three-dimensional numerical example, i.e. the simulation of a thick-walled two-layered artery-like tube subjected to internal pressure and residual stresses. The highly non-linear elastic behaviour of the material is well reflected by the mechanical response of the tube within the physiological pressure range. For higher pressure values the material softens significantly, deviates from the elastic path and finally drops towards the elastic response of the undamaged neo-Hookean ground substance. Physically, this can be interpreted as a continuous degradation of the fibres contained in an undamaged matrix material. The damage evolution beyond the physiological range results in an increase of the tube's diameter at the same mean pressure. Consequently, at the expense of a loss in stiffness, these damage effects can be beneficially used in medical surgery to expand an artery's diameter and thereby restore the blood flow in atherosclerotic blood vessels for example. As an interesting consequence of the residual stresses and the related homogenised stress distribution over the tube thickness, we observe an increase of the peak pressure before the overall structural response enters the unloading path. In other words, due to the presence of residual stresses, arteries are able to sustain higher supraphysiological loads. This illustratively shows the beneficial impact of residual stresses on the overall behaviour of arteries.

It is important to mention that the assumption of an intact matrix and two equally damaging fibre families provides only a limited view of the real (bio)mechanical effects at this stage. Therefore, ongoing research work aims at extending the formulation to three global damage variables, including matrix-damage and individual damage for each fibre family.

References

1. Aifantis, E.: On the role of gradients in the localization of deformation and fracture. *Int. J. Eng. Sci.* **30**, 1279–1299 (1992)
2. Dimitrijević, B.J., Hackl, K.: A method for gradient enhancement of continuum damage models. *Technische Mechanik* **28**, 43–52 (2008)
3. Eringen, A. (ed.): *Continuum Physics. Volume IV—Polar and Nonlocal Field Theories*. Academic Press, New York (1976)
4. Eringen, A.: *Nonlocal Continuum Field Theories*. Springer, New York (2002)
5. Gasser, T., Ogden, R., Holzapfel, G.: Hyperelastic modelling of arterial layers with distributed collagen fibre orientations. *J. R. Soc. Interface* **3**, 15–35 (2006)
6. Holzapfel, G., Gasser, T., Ogden, R.: A new constitutive framework for arterial wall mechanics and a comparative study of material models. *J. Elast.* **61**, 1–48 (2000)
7. Johnson, B., Hoger, A.: The use of virtual configuration in formulating constitutive equations for residually stressed elastic materials. *J. Elast.* **41**, 177–215 (1995)
8. Kachanov, L.: Time of the rupture process under creep conditions. *Izvestija Akademii Nauk Sojuza Sovetskikh Socialisticheskikh Respubliki (SSSR) Otdelenie Technicheskikh Nauk (Moskra)* vol. 8, pp. 26–31 (1958)
9. Krajcinovic, D., Lemaitre, J.: *Continuum Damage Mechanics. CISM Courses and Lectures*, vol. 295. Springer, New York (1987)
10. Lemaitre, J.: *A Course on Damage Mechanics*, 2nd edn. Springer, Berlin (1996)
11. Liebe, T., Steinmann, P., Benallal, A.: Theoretical and computational aspects of a thermodynamically consistent framework for geometrically linear gradient damage. *Comput. Methods Appl. Mech. Eng.* **190**, 6555–6576 (2001)
12. Menzel, A., Harrysson, M., Ristinmaa, M.: Towards an orientation-distribution-based multi-scale approach for remodelling biological tissues. *Comput. Methods Biomech. Biomed. Eng.* **11**, 505–524 (2008)
13. Rogula, D. (ed.): *Nonlocal Theory of Material Media. CISM Courses and Lectures*, vol. 268. Springer, New York (1982)
14. Waffenschmidt, T.: *Modelling and simulation of adaptation and degradation in anisotropic biological tissues*. Ph.D. Thesis. Institut für Mechanik, Technische Universität Dortmund (2014). <http://hdl.handle.net/2003/31797>
15. Waffenschmidt, T., Menzel, A.: Extremal states of energy of a double-layered thick-walled tube—application to residually stressed arteries. *J. Mech. Behav. Biomed. Mater.* **29**, 635–654 (2014)
16. Waffenschmidt, T., Polindara, C., Menzel, A., Blanco, S.: A gradient-enhanced large-deformation continuum damage model for fibre-reinforced materials. *Comput. Methods Appl. Mech. Eng.* **268**, 801–842 (2014)

Biomedical Technology

Lenarz, Th.; Wriggers, P. (Eds.)

2015, VIII, 187 p. 92 illus., 53 illus. in color., Hardcover

ISBN: 978-3-319-10980-0